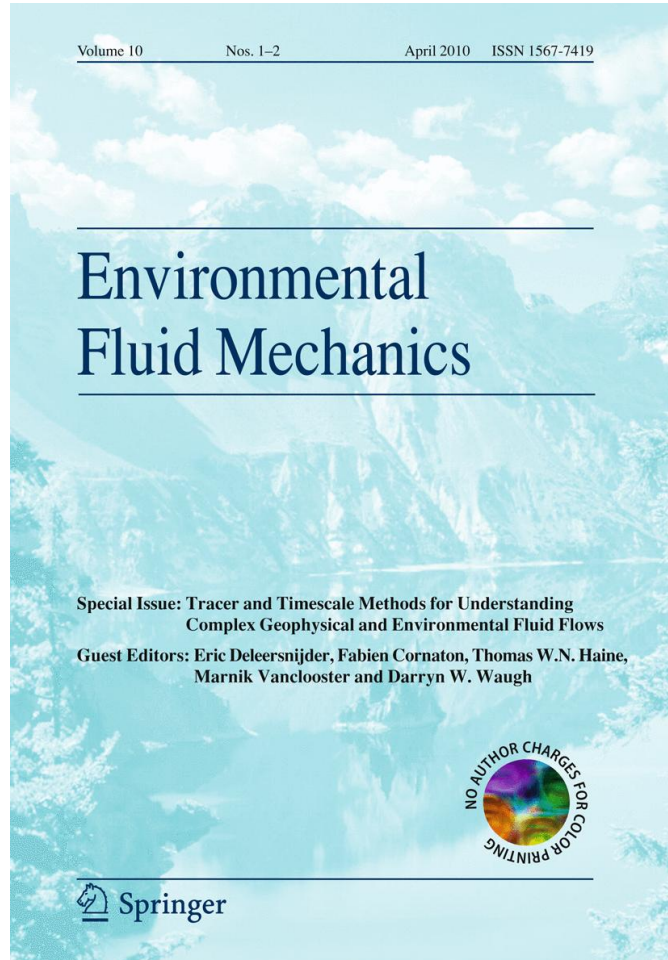


ISSN 1567-7419, Volume 10, Combined 1-2



**This article was published in the above mentioned Springer issue.
The material, including all portions thereof, is protected by copyright;
all rights are held exclusively by Springer Science + Business Media.
The material is for personal use only;
commercial use is not permitted.
Unauthorized reproduction, transfer and/or use
may be a violation of criminal as well as civil law.**

Helium isotopic constraints on simulated ocean circulations: implications for abyssal theories

Jean-Claude Dutay · Julien Emile-Geay ·
Daniele Iudicone · Philippe Jean-Baptiste ·
Gurvan Madec · Claire Carouge

Received: 13 November 2008 / Accepted: 18 November 2009 / Published online: 18 December 2009
© Springer Science+Business Media B.V. 2009

Abstract There is ongoing controversy as to the dynamical significance of geothermal heat flow in shaping the abyssal circulation. In this paper, we gauge the impact of geothermal heating and vertical mixing parameterizations in the general circulation model OPA. The experiments are evaluated by comparing simulated mantle ^3He with observations collected during the GEOSECS and WOCE programs. This tracer is particularly adapted to the validation of our numerical simulations because its injection into the ocean interior is tightly linked to geothermal processes. In agreement with previous studies, the model circulation is found very sensitive to the parameterization of the vertical mixing. The meridional overturning circulation (MOC) is globally intensified when moving from a constant mixing to a version with enhanced mixing near the ocean bottom, with the most drastic variation observed for AABW (+50%). Adding the geothermal heat flux mainly affects AABW circulation in the model, enhancing it all the more as the meridional circulation is slow (low vertical mixing), but proportionally less so when it is more vigorous (enhanced vertical mixing). This can be understood from the requirement of the abyssal ocean to maintain heat balance. The evaluation with mantle ^3He simulations reveals that the version with low vertical mixing, with its sluggish circulation, produces unrealistically high a ^3He isotopic composition. However, with a vertical mixing that is enhanced at depth, the ^3He distribution falls within an acceptable range of values in the deep ocean. Finally, adding the geothermal heating to this enhanced mixing case provides a substantial improvement of the simulation of AABW in all basins but

J.-C. Dutay (✉) · P. Jean-Baptiste · C. Carouge
LSCE, IPSL/CEA, UVSQ, CNRS, Gif sur Yvette, France
e-mail: jean-claude.dutay@lsce.ipsl.fr

J. Emile-Geay
Department of Earth Sciences, University of Southern California, Los Angeles, CA, USA
e-mail: julieneg@usc.edu

D. Iudicone · G. Madec
IPSL/LOCEAN, Paris, France

D. Iudicone
Stazione Zoologica “Anton Dohrn”, Naples, Italy

the Indian Ocean. ^3He isotopic composition is then in good agreement with the observations. Taken jointly with observational estimates of the MOC intensity, these independent isotopic constraints suggest that both geothermal heating and enhanced diapycnal mixing at depth are key ingredients in the realistic simulation of abyssal circulation.

Keywords Ocean · Tracer · Helium-3 · Geothermal flux · Model

1 Introduction

The ocean circulation plays an important role in climate variability, e.g. [40,53], with the ocean having a great capacity to store and transport heat and CO_2 , as well as exchanging these with the atmosphere. Thus it contributes significantly to the poleward transfer of excess solar energy received in the low latitudes to higher latitudes. In addition, it governs atmospheric CO_2 concentrations, since it contains about 50 times more CO_2 than the atmosphere, with the majority in the deep ocean [6]. Hence, understanding the dynamics of the deep-ocean is essential to the study of global climate change, via the carbon cycle.

Ocean general circulation models (OGCMs) provide the only controllable environment with which to answer such questions. It is thus crucial to understand the processes and forcings that control the strength and patterns of the simulated deep-ocean circulation. Many previous studies have shown the importance of the parameterization of small-scale mixing processes on ocean circulation [9, 10, 16, 35, 58]. Indeed, the models' deep-ocean circulation are known to be particularly sensitive to the vertical mixing parameterization [7, 54]. Since the deep ocean is essentially aphotic, diapycnal mixing is chiefly responsible for the transfer of water mass characteristics from top to bottom away from convective regions (i.e. over much of the global ocean), thereby mapping surface density gradients onto the deep ocean. These gradients, in turn, support the abyssal circulation via geostrophic balance.

There is, however, another process supplying heat to the abyss. Although it has long been neglected by oceanographers, e.g. [26], geothermal heating has recently been recognized as a significant actor in abyssal dynamics and thermodynamics [1, 2, 13, 45, 52].

While its magnitude is small compared to surface heat fluxes, geothermal heating acts on a much broader area—the entire seafloor. Overall, it contributes a comparable amount of buoyancy to bottom waters as air/sea fluxes—albeit of opposite sign over the Southern Ocean. Furthermore, it acts below the thermocline, in regions of the ocean where small thermal gradients mean that the downward diffusive heat flux is also small. So small, in fact, as to be commensurate to geothermal heat flow over much of the seafloor's surface [13]. As a result, the same authors found a realistic representation of geothermal heating was able to generate a deep circulation of the order of several Sverdrups¹ for Antarctic Bottom Water (AABW), and suggested that it constitutes a driving force of the AABW cell. This statement must be tempered by the observation that the deep circulation response to geothermal forcing is much reduced when diapycnal mixing is very strong—as appears to be the case in the vicinity of rough topography. Nonetheless, the convergence of idealized [1, 45, 52] and more realistic [13] studies of its impact justifies the claim that geothermal heat flow significantly shapes the abyssal circulation. Can these model-based theories be substantiated by observational constraints?

In this paper we use ^3He tracer data to evaluate the suite of modeling experiments. The model circulation is used to simulate natural ^3He distributions and compare them to obser-

¹ 1 Sverdrup (Sv) = $10^6 \text{ m}^3 \text{ s}^{-1}$.

vations. This inert tracer, whose oceanic behavior is tightly linked to geothermal heat flow [25], is particularly apt to probing the effect of geothermal heat flow on the model's deep circulation. Indeed, its source consists of mantle ^3He that is injected into the oceans by the hydrothermal circulation at deep sea spreading ridges, where most of the geothermal heat flux is also transferred to the ocean [8, 31, 44]. This injection of hot hydrothermal fluids enriched in ^3He produces large scale ^3He plumes (with ^3He excesses up to 30–40% relative to the solubility equilibrium with the atmosphere), that are dispersed by the prevailing currents and can be used for tracing deep ocean currents and for evaluating ocean general circulation model [12, 17]. The comparison from six OGCM during the Ocean Carbon Model Intercomparison Project (OCMIP2) has shown that the modeled ^3He distribution is very sensitive to the simulated circulation and that the parameterization proposed by Farley et al. [17] for its source function is robust [12]. During OCMIP-2, six different global OGCMs were tested with mantle ^3He simulations [12]. This inter-comparison has revealed that the resulting circulation was a direct consequence of the models' characteristics. More precisely, the OGCMs coupled to a sea-ice model were found to produce a substantial amount of bottom water in the Southern Ocean, which tended to overestimate AABW ventilation and to produce too low a ^3He value in this region. Conversely, models that were not coupled with a sea-ice model were systematically underestimating AABW ventilation and simulating excessive ^3He values. Moreover, the parameterization of sub-grid scale mixing (which is recognized to generate large effect on the simulated circulation and tracer redistribution, e.g. [14]) also accounted for significant discrepancies. The two OCMIP2 models coupled to a sea-ice model were not using the eddy-induced velocity parameterization of Gent et al. [20]. Sensitivity tests performed during that project clearly demonstrated that this parameterization tended to reduce ventilation of the deep ocean, and to generate higher ^3He excesses. The wide range of simulated distributions during OCMIP2 has been a motivation to explore in more details the impact of the physics on the modeled deep ocean circulation and to further evaluate it with mantle ^3He simulations. Taking into account the experience gained during the OCMIP2 exercise, we have initiated our new modeling efforts with a more recent configuration of the OPA model with characteristics that provide a more realistic circulation. This analysis focuses on the impact of the geothermal heating and the parameterization of the vertical mixing on the circulation simulated by the model.

2 Description of the model and the simulations

The ice-ocean coupled model is OPA, developed at IPSL/LOCEAN [33], in its global configuration ORCA2-LIM. The horizontal mesh is based on a 2° by 1.5° Mercator grid. It has been modified poleward of 20°N in order to include two numerical inland poles and meridional resolution is refined up to 0.5° at the equator [32]. There are 31 vertical levels, with the highest resolution (10 m) in the upper 150 m. The upper boundary uses a free surface formulation [42]. The model is coupled to the dynamical-thermodynamical sea ice model LIM [21]. Lateral mixing is performed along isopycnal surfaces, and the eddy-induced velocity parameterization of Gent and McWilliams (1990) is added. The vertical mixing scheme uses a turbulent closure [4], and a diffusive bottom boundary layer parameterization [3] is included.

Two versions of the model background vertical diffusivity are tested in our simulations. A first version (CONTROL) uses a constant values of $0.12 \times 10^{-4} \text{ m}^2 \text{ s}^{-1}$ throughout the entire ocean volume, and a second version (High K_z) where it increases linearly from the surface to the bottom in order to mimic the effects of decreased stratification and increased

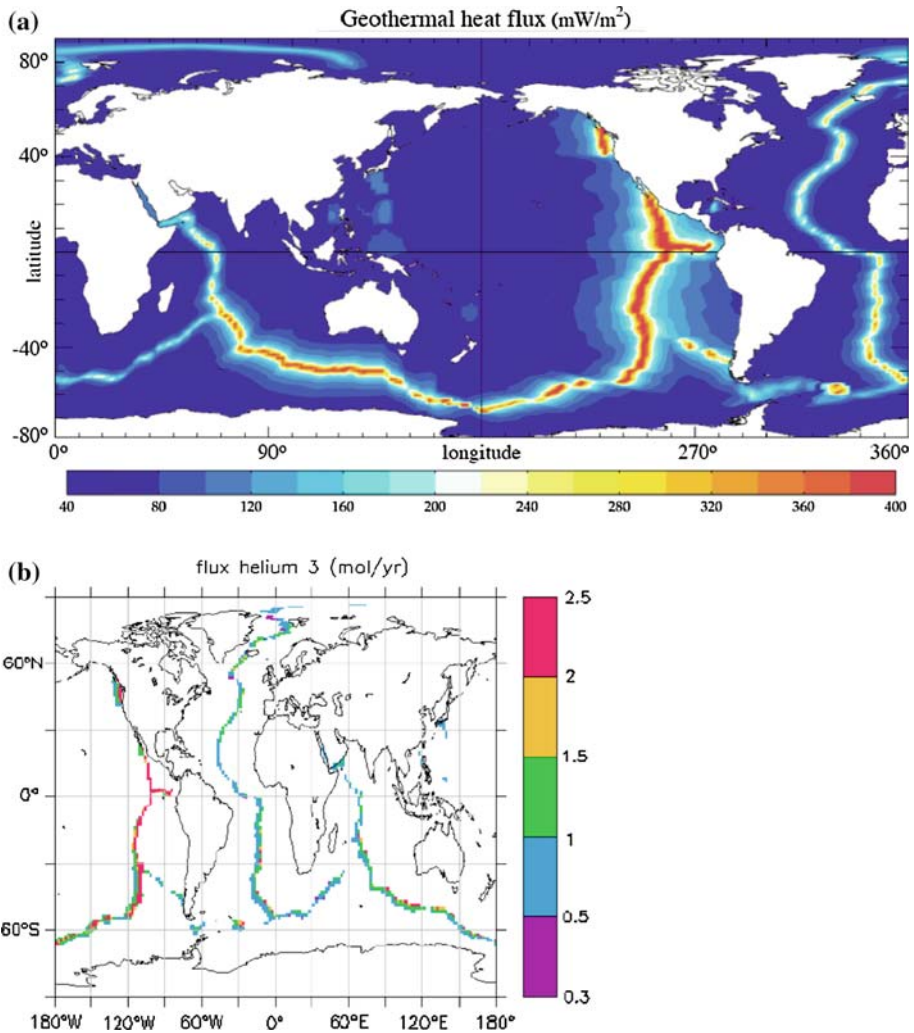


Fig. 1 **a** Geothermal heat flux (units: mW m^{-2}), **b** mantle helium-3 flux (units: mol year^{-1})

small-scale turbulence near the bottom (values ranges from $0.12 \times 10^{-4} \text{ m}^2 \text{ s}^{-1}$ in the first 1000 m to $1.2 \times 10^{-4} \text{ m}^2 \text{ s}^{-1}$ at depth).

At the surface, the model is forced by fluxes of heat and freshwater prescribed with bulk formulae using monthly climatologies. A penetrative shortwave solar radiation formulation is used. A restoring to climatological surface salinities was also added, that is only significant in the North Atlantic and Greenland Sea. Climatological ERS1/2 scatterometer monthly mean wind stresses were used for the tropics while the NCEP/NCAR climatology was used poleward of 50°N and 50°S .

At the bottom, we include in some experiments the geothermal heating term (Q_{geo}) developed by Emile-Geay and Madec [13], who parameterized the heat source as a function of the age of the bedrock. The global mean value is 86.4 mW m^{-2} , close to observational estimates [48]. Its spatial distribution is shown in Fig. 1a, which closely mirrors seafloor age [34]. The

Table 1 Mean $\delta^3\text{He}$ value (units: ‰)

	Global	Atlantic	Pacific	Indian	Southern Ocean (south of 45°S)
Exp 1: Control	8.5	5.6	15.6	11.7	9.8
Exp 2: Q_{geo}	7.8 (8)	4.7 (16)	14.5 (7)	10.8 (8)	8.6 (12)
Exp 3: High K_z	6.2 (27)	3.5 (38)	11.9 (23)	8.8 (25)	6.4 (35)
Exp 4: Q_{geo} + High K_z	5.7 (32)	3.0 (46)	11.0 (29)	8.0 (32)	5.5 (44)

Values in brackets correspond to the percentage of variation with the control experiment

highest values are observed along the ridge system where the lithosphere formed at high temperature, then was displaced outward by lithospheric plate divergence. Along ridge axes, geothermal heat flux is directly related to the spreading rates: maxima are located in the eastern Pacific Ocean, where the spreading rate is highest; lowest values are observed in the Atlantic, with intermediate values in the Indian and Southern Oceans.

We have performed four simulations in order to investigate the sensitivity of the ocean circulation to both vertical mixing parameterization and geothermal heating (Table 1). Our first experiment (CONTROL) uses a constant vertical mixing coefficient and the geothermal forcing is not included. In the second experiment (Q_{geo}), the geothermal heating is added. The third experiment (High K_z) does not include geothermal heating, but has a vertical mixing parameterization with values increasing with depth (see Sect. 2). The fourth experiment includes both geothermal heating and the vertical mixing coefficient that varies with depth (exp 4 = High K_z + Q_{geo}). This last experiment has been extensively evaluated and analyzed in detail in Iudicone et al. [22,23].

3 Global meridional stream functions

We first analyze the global meridional stream functions of the different experiments. In the control experiment, the circulation associated with the North Atlantic deep water overturning (NADW) (between 1000 and 2500 m depth) reaches 15 Sv, and below 3000 m the circulation related to the AABW is on the order of 5 Sv (Fig. 2). These diagnostics are not easily constrained by the observations, as diagnosed stream functions or transports usually carry large uncertainties (3–5 Sv, [50]). However, the mean strength of the NADW in the Atlantic Ocean overturning is comparable to observational estimates, 18 ± 5 Sv [50] and 16 ± 3 Sv [18]. In contrast, the AABW circulation seems weak: using geochemical tracers budgets Orsi et al. [37] estimated the ventilation of AABW on shelves of Antarctica to be 8–10 Sv, and global AABW overturning is estimated from hydrographic data to be 22 Sv [50]. Adding the influence of geothermal heating (exp 2), the main adjustment is an increase of 50% in the strength of the AABW cell (Fig. 2). Conversely, a quasi-insignificant change is observed for the NADW cell. These variations are necessary to compensate for the additional heat supplied to the abyssal ocean [45]. It affects predominantly AABW because the geothermal heating is injected at the ocean floor and only weakly affects the shallower NADW. In addition, the magnitude of geothermal heating is smallest in the Atlantic Ocean. In the third experiment, when the vertical mixing increases with depth, the thermohaline circulation is enhanced. In comparison to the control run (exp 1), the strength of the AABW cell is doubled (to 10 Sv), and the NADW cell increases to 17.5 Sv (+17%). This large increase in the thermohaline circulation is due to the more efficient vertical transfer of the characteristics of the water

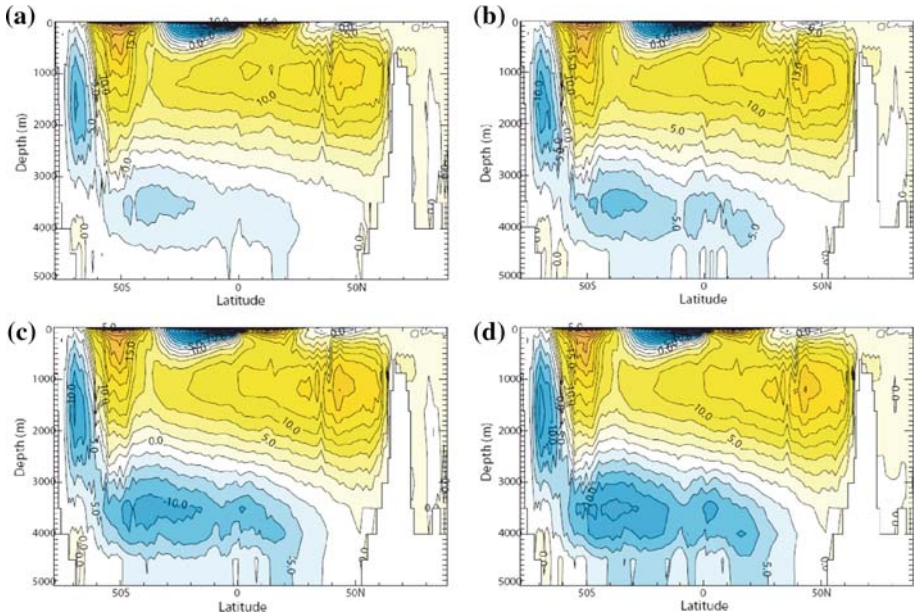


Fig. 2 Global meridional stream functions (units: Sv; $1 \text{ Sv} = 10^6 \text{ m}^3 \text{ s}^{-1}$). **a** Exp 1, **b** exp 2, **c** exp 3, **d** exp 4

masses produced in the surface layer, which magnifies density gradients in the deep ocean and produces a more intense circulation via geostrophy.

Including the geothermal heating in the version with high vertical mixing leads to almost no change in NADW, but an additional increase of 1.8 Sv (+17.5%) for the AABW cell. The variation obtained by including the geothermal forcing is smaller than for the control run (exp 2 versus exp 1) because the high diapycnal mixing produces an abyssal circulation that is already more vigorous and hence more efficient at transporting heat. This causes only a modest increase in circulation to compensate for the geothermal heat injected at depth and keep the deep ocean in thermal equilibrium [13].

In the model, about 5 Sv of extremely dense Antarctic shelf water converges into the AABW class [22] and is subsequently transformed by the model bottom boundary layer parameterization, which mimics the dense gravity currents descending the slopes of Antarctica to produce AABW. This process is not well simulated because of the excessive lateral diffusion which dilutes the water mass before it reaches the ocean bottom, as occurs in the majority of coarse resolution OGCMs. The result is an AABW strength at 30°S of about 10 Sv, weaker than most observational estimates, e.g., [46, 50]. The export of bottom waters toward the Pacific Basin is similar to the estimate in Talley et al. [50]. The CDW import is 50% weaker than observed and so too is AABW export, though observational estimates can vary by as much as 50 Sv [22, 23]. The overturning of deep and bottom water in the Indian basin (about 3 Sv) is largely underestimated compared to estimates from inverse models, which range from 7 [19] to 24 Sv [43] (see [50] for a discussion). The model's deep circulation in the Atlantic basin is the closest to observations: NADW/CDW at 30°S is 17.1 Sv in the model as compared to 17.8 Sv in Talley et al. [50], AABW is 2.8 Sv in the model relative to 3.8 Sv in Talley et al. [50] and 6 Sv in Sloyan and Rintoul [46].

Recent studies on the dynamics of the AABW transport have proposed that AABW in the Atlantic Ocean is sensitive to the surface salinity along the Antarctic coast [39] and mixing by lateral diffusion [27]. In this context the model intercomparison study by Weber et al. [56] on the MOC during glacial periods gives interesting indications on the dynamics of the bottom cell. They found that the bottom overturning scales well with both the deep meridional density contrast and—as proposed by Kamenkovich and Goodman [27]—the vertical extent of the deep cell.

From the analysis of our global simulations a complex picture of the sensitivity of AABW to deep mixing emerged, whose main features are summarized here (a more detailed discussion will be presented in a separate manuscript (Iudicone et al., in preparation)).

The most relevant results are related to the Southern Ocean overturning of NADW, which is extremely high and weakly dependent on the deep mixing intensity (in both cases about 80% of NADW is transformed into other water masses). The difference lies in the partitioning of NADW into bottom (AABW) and subsurface waters (SAMW, AAIW). A lower (higher) deep mixing generates a larger (lower) upwelling and a lower (higher) downwelling, which in turn corresponds to a shallower (deeper) separation between the upper and bottom overturning cells.

Furthermore, in the case of low deep diffusivity, most of the weakening of the AABW cell is associated with a reduced deep upwelling in the Pacific basin while the inflow into the Indian Ocean is less affected. In the Atlantic Ocean, a reduced northward penetration of AABW is observed together with a deepening of NADW, in good agreement with the theory of Kamenkovich and Goodman [27]. Interestingly, the flow of AABW through the Drake Passage is also strongly affected, with a transport that largely exceeds observational estimates in the case of low diffusivity. Therefore an intense vertical mixing is necessary to reproduce the vertical water mass distribution in the Southern Ocean, as suggested also by observations, e.g. [36].

In principle, the effect of deep mixing on AABW is not limited to a direct influence on the deep and bottom stratification. First, the Southern Ocean upwelling maps the deep anomalies onto the sub-surface water masses. Therefore, deep mixing can also influence the properties of AABW by altering the water mass properties at the surface and thus it can in principle feedback onto AABW formation. This can be particularly true for salinity, which dominates the density variations at low temperatures. However, the role of this latter process could not be fully evaluated in our simulations. Indeed, in our ocean-forced simulations, even in presence of a sea-ice model, the subsurface emergence of deep salinity anomalies in the Southern Ocean is somewhat damped by partially restoring to climatological values.

The other indirect impact of deep diffusivity on AABW formation is related to the overflow mechanism. After surface AABW formation, these very cold waters cascade along the continental slopes of Antarctica. In this process, shear and thermobaric processes increase the volume of dense water by promoting mixing with the incoming NADW, whose thermohaline properties depend on the same diffusivity.

In summary, deep diffusivity impacts the AABW distribution in the ocean by altering both the water mass formation and consumption rates (see discussion in [23]). For the reasons discussed above, only fully coupled ocean-atmosphere-sea-ice models allow for a thorough exploration of the sensitivity of AABW to diapycnal mixing. In particular, the impact of regional mixing variability will be left for future study.

These results illustrate the sensitivity of the model to the parameterization of vertical mixing and geothermal forcing. We will now evaluate the impact of these changes with natural ^3He simulations.

4 Natural ^3He simulations

4.1 Parameterization of mantle helium injection

The four simulations used the same parameterization for mantle helium injection. The protocol is very similar to that proposed by Farley et al. [17], and further validated using simulations from six OGCM during OCMIP-2 [12]. We simulate both ^3He and ^4He distributions, and mantle ^3He is injected along ocean ridges with an isotopic ratio ($\delta^3\text{He}^2$) of 700‰. It is injected at a global rate of 1000 mol $^3\text{He}/\text{year}$ at 300 m above the ridge axis. $\delta^3\text{He}$ is next calculated from the outputs of the simulation (^3He and ^4He concentrations) using its classical definition. The only difference with the OCMIP-2 protocol (<http://www.ipsl.jussieu.fr/OCMIP/>) is that the mantle helium flux along the ridge axis is proportional to the geothermal flux, instead to be proportional to the ridge spreading rate. This adaptation, formulated for better consistency with the dynamical forcing of our model, induces no significant changes for the spatial distribution of the mantle helium source in the ocean. The depth of injection varies between 2000 and 3000 m. Maximum fluxes occur in the Pacific Ocean at the East Pacific Rise (EPR), intermediate fluxes are found in the Indian and Southern Oceans, while minimum fluxes are associated with the Mid-Atlantic Ridge (MAR) (Fig. 1b). The only sink for mantle helium is loss to the atmosphere, which is prescribed using the gas exchange formulation of Wanninkhof [55] (<http://www.ipsl.jussieu.fr/OCMIP/>). Simulations are integrated off-line until they reached a quasi-steady state when the globally integrated ^3He drift were less than 4 mol year $^{-1}$.

4.2 Results

The horizontal distributions of the depth-averaged tracer distributions provide a global description of the performance of the simulations (Fig. 3). The inter-basin tracer distribution is qualitatively similar among the simulations. The highest $\delta^3\text{He}$ values are found in the Pacific Ocean where the rate of injection is the most elevated (Fig. 1b), and no newly ventilated deep water is formed. The zonal contrast is important facet of this basin, with high ^3He values simulated close to the East Pacific Rise where the mantle helium flux reaches a maximum. The lowest $\delta^3\text{He}$ values are simulated in the Atlantic Ocean where the rate of injection is the lowest, and recently ventilated NADW waters with a low $\delta^3\text{He}$ value are overflowing. In the Indian and southern Ocean, where the rate of tracer injection is intermediate, $\delta^3\text{He}$ values are in between those simulated in the Pacific and Atlantic basins. Still lower values are observed in the Southern ocean where upwelling in the Antarctic Circumpolar Current (ACC) tends to remove helium by bringing it to the surface where it degasses to the atmosphere. However, large quantitative differences are observed in $\delta^3\text{He}$ among the simulations, illustrating the large sensitivity of this tracer to the ocean circulation. Modeled $\delta^3\text{He}$ values are straightforwardly interpreted as a function of the strength of meridional overturning circulation. The control experiment with the weakest overturning circulation (Fig. 2), features a longer residence time of the tracer in the ocean (Table 2) and the highest simulated $\delta^3\text{He}$ values. The increase in meridional overturning simulated in the other experiments acts to reduce the residence time of the tracer in the ocean (Table 2) and generates globally lower $\delta^3\text{He}$ values (Table 1). The global mean ^3He isotopic composition is reduced by 8, 27 and 32%, respectively, from exp 2 to exp 4 (Table 2). These percentages are also more elevated in the

² $\delta^3\text{He} = 100((R_{\text{ocean}}/R_{\text{atmosphere}}) - 1)$ and $R = ^3\text{He}/^4\text{He}$.

depth averaged helium3 isotopic composition

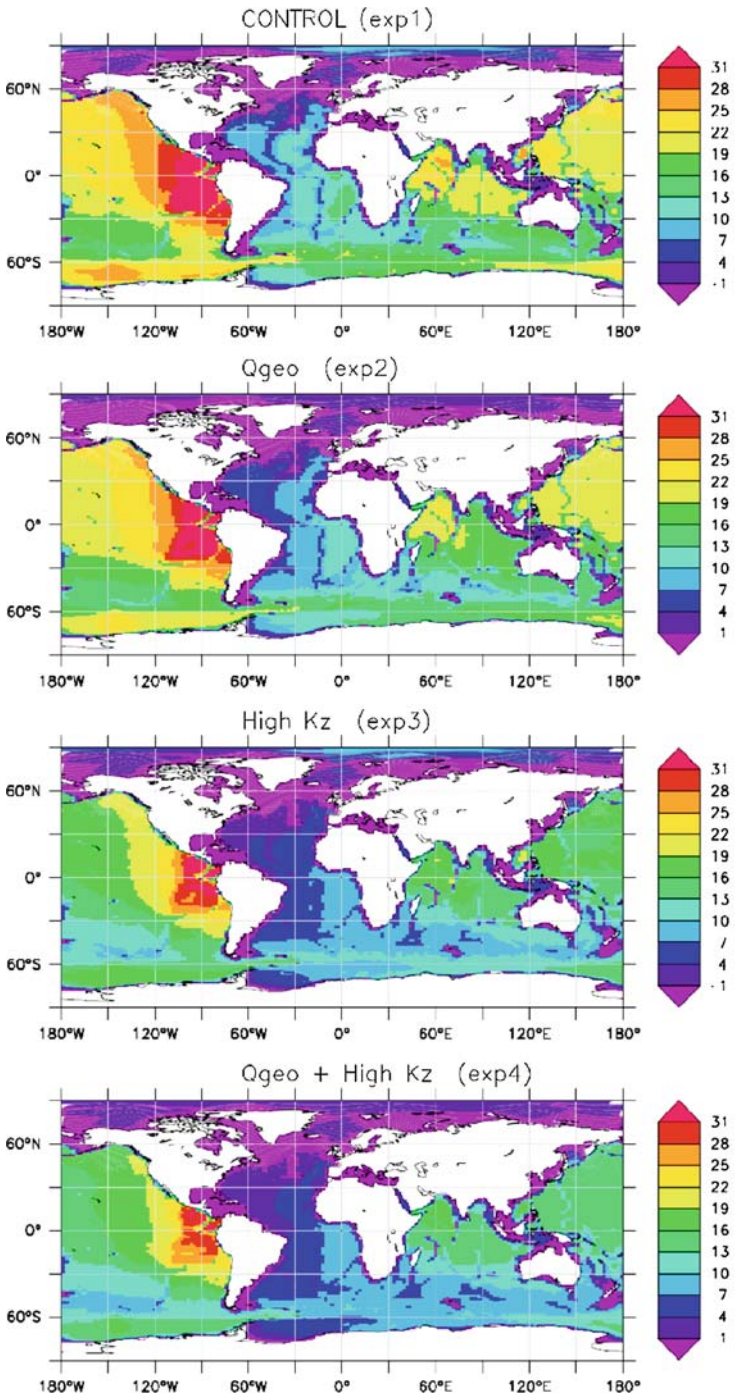


Fig. 3 Depth averaged helium-3 isotopic composition (units: %)

Table 2 Mantle ^3He residence time (units: year) defined as the ratio of the global mantle ^3He inventory to the mantle ^3He source

	^3He residence time
Exp 1: Control	855
Exp 2: Q_{geo}	789
Exp 3: High K_z	651
Exp 4: Q_{geo} +High K_z	604

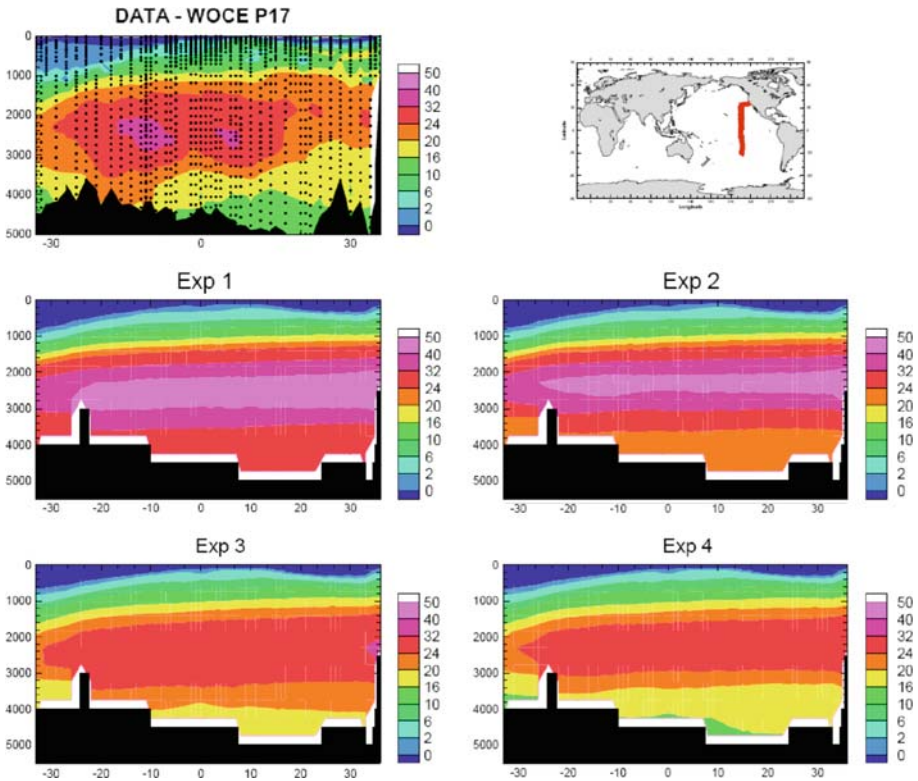


Fig. 4 Observed and simulated helium-3 isotopic composition along the WOCE P17 section in the Pacific Ocean (units: %)

Atlantic and Southern Ocean, where deep waters are formed and ^3He isotopic composition is lower.

An opportunity to evaluate the simulated natural ^3He distributions is provided by the data collected during the GEOSECS and WOCE programs (http://www.ldeo.columbia.edu/res/fac/etg/text/woce_data.html) [29,30,44,47,57]. Model outputs are compared with observations along the WOCE P17 and WOCE P04 in the Pacific Ocean (Figs. 4, 5), the GEOSECS section in the Atlantic Ocean (Fig. 6) and the WOCE I07 sections in the Indian Ocean (Fig. 7). In the Pacific Ocean, the control experiment (exp 1) has ^3He isotopic compositions which are largely overestimated compared to the two WOCE sections (Figs. 4, 5). The weak circulation generated in this experiment produces $\delta^3\text{He}$ values almost twice as large as those observed. When geothermal heating is added in the second experiment, $\delta^3\text{He}$ values are globally reduced. The variations are most noticeable below 3000 m in the AABW cell, where modeled values

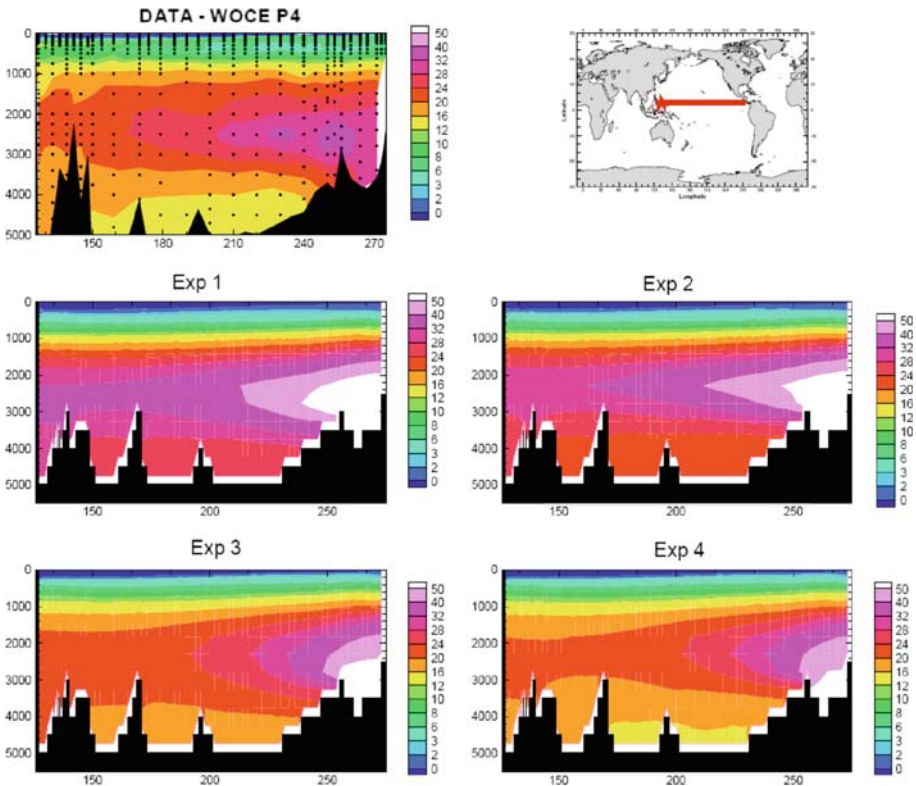


Fig. 5 Observed and simulated helium-3 isotopic composition along the WOCE P4 section in the Pacific Ocean (units: ‰)

are reduced by 20%, but still remain too high relative to the observations. Changes in $\delta^3\text{He}$ isotopic composition are still more pronounced when vertical mixing is increased (exp 3). The reduction in $\delta^3\text{He}$ values is again globally accentuated, with a substantial decrease now also occurring in the deep and intermediate water (1000, 3000 m) near the tracer injection depth. These changes lead to a range of modeled $\delta^3\text{He}$ values now comparable to observations in the Pacific Ocean. When geothermal forcing is added to the version with high vertical mixing (exp 4), very pronounced changes again occur in the simulated bottom waters. The simulated $\delta^3\text{He}$ isotopic compositions then compare much more favorably to observations along each section, especially for AABW. There however remain discrepancies in the simulations that are generally attributable to the coarse resolution of the model. The westward propagation of the enriched $\delta^3\text{He}$ plume is too weak (Fig. 4) and the two $\delta^3\text{He}$ maxima associated with plume jets on both sides of the equator are not simulated (Fig. 5).

In general, a comparison to observations reveals similar performances in other basins. The progressive decrease of simulated $\delta^3\text{He}$ values following the evolution of the configuration of the model observed in the Pacific Ocean, is found again in the Indian Ocean (Fig. 7). However, if the modeled $\delta^3\text{He}$ values are globally reduced from exp 1 to exp 4, they remain, in general, largely overestimated compared to the observations, especially at mid-depth where the tracer is injected. The only water mass showing a realistic improvement in $\delta^3\text{He}$ isotopic composition is AABW, which is quite realistic in exp 4.

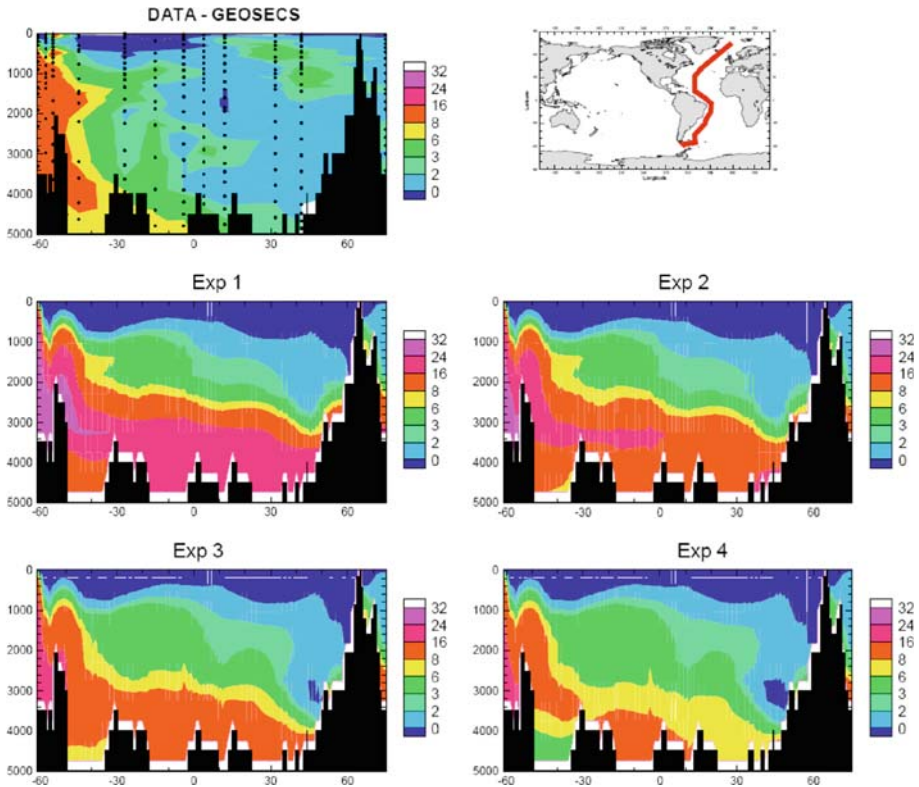


Fig. 6 Observed and simulated helium-3 isotopic composition along the GEOSECS section in the Atlantic Ocean (units: ‰)

In the Atlantic Ocean where model sensitivity is most pronounced (Table 1), comparison with the GEOSECS observations (Fig. 7) reveals that the main improvement among the different simulations occurs for bottom waters flowing from the Southern Ocean. Large variations are observed in the AABW helium isotopic composition, with the control experiment displaying a higher bias here than in other basins. A noticeable improvement is observed in the Antarctic Circumpolar Current (ACC) for the experiments with higher vertical mixing (exp 3 and exp 4), that is in turn propagated through the AABW isotopic signature and provides more realistic values compared to bottom water observations. This is especially true of the last experiment where geothermal forcing is included (exp 4). Conversely, all simulations successfully produce a realistic helium isotopic composition at depth in the North Atlantic Ocean close to the formation region of NADW. However, NADW gets inconsistently enriched in ^3He during its southward journey through the Deep Western Boundary Current, in a generally similar fashion for all simulations.

5 Discussion

It is clear that the main reason for the discrepancies between the control simulation and observations is an excessively weak abyssal circulation, especially for bottom water. Though

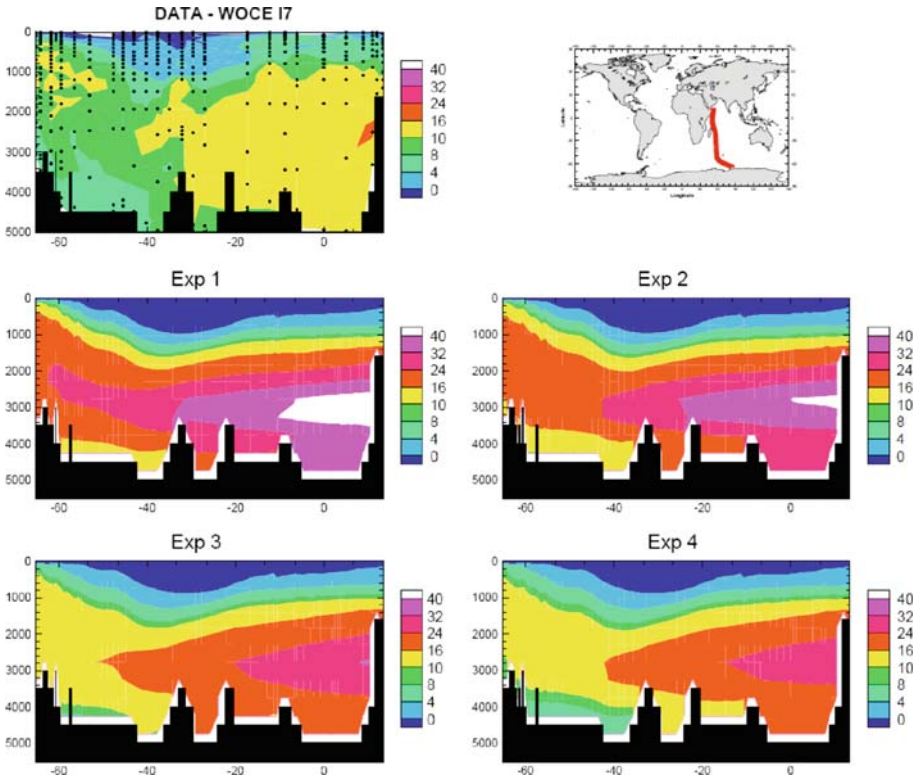


Fig. 7 Observed and simulated helium-3 isotopic composition along the WOCE I7 section in the Indian Ocean (units: ‰)

modeled NADW overturning in exp 1 (15 Sv) ranks close to the lower limit of a variety of observationally-based estimations (13–15 Sv in [18], 12–23 Sv in [45], 18 Sv in [50]), the intensity of the simulated AABW cell (2.5 Sv) is far below observational estimates (5–8 Sv production rate [37], 22 Sv [50]). This sluggish circulation generates a long ^3He residence time and unrealistic isotopic mantle ^3He values that largely exceed the observations. The slow circulation is due in part to the weak vertical mixing prescribed throughout the water column. The value of the mixing coefficient ($0.1 \text{ cm}^2 \text{ s}^{-1}$) is adequate for the thermocline—where stratification is strong by definition—but inadequate for bottom water where greater mixing is observed, especially in oceanic regions of rough topography [24].

The modeled thermohaline circulation can be strengthened by increasing vertical mixing as suggested by Bryan [7], but also by including geothermal flux as a forcing, as first suggested by Adcroft et al. [1]. Here we have evaluated in more detail the impact of these two processes on the ocean circulation with mantle ^3He simulation.

Adding the geothermal heat flux (exp 2) strengthens the AABW cell, but has little impact on the circulation above 3000 m depth (Fig. 2). When compared to the control experiment, this simulation leads to unrealistically high $\delta^3\text{He}$ values above 3000 m depth. While the intensity of the AABW cell is increased (5 Sv), it is still too moderate to provide a realistic range of helium isotopic composition near the bottom. We find that changing the vertical mixing parameterization to a version where mixing is enhanced in the deep ocean

globally improves the model's performance (exp 3). The overturning circulation and the simulated $\delta^3\text{He}$ values are both adjusted towards more realistic values. The improvement in AABW is more significant than when including the geothermal heating alone, even if near-bottom $\delta^3\text{He}$ values remain slightly too high. Increasing vertical mixing leads to noticeable improvement in the simulation at mid-depth in the ocean where the tracer is injected. Deep ocean ventilation is then improved to the point of simulating a realistic range of $\delta^3\text{He}$ values where the enriched plumes of mantle helium are observed.

When the geothermal heating is added to the version with high vertical mixing (exp 4) the relative change is less intense than when the mixing was low (exp 1/exp 2) because the deep ocean circulation is already vigorous enough to readily remove the additional heating injected at the bottom [1,45]. Equivalently, strong diapycnal mixing generates important lateral temperature gradients at depth by mapping surface density patterns onto the bottom. The simple scaling law of Emile-Geay and Madec [13] (their Eq. 11) explains why only a small increase in circulation is then necessary to keep the deep ocean in thermal equilibrium for a given geothermal input.

This small circulation change notwithstanding, a noticeable additional improvement is observed on the distribution of isotopic mantle helium in AABW, where $\delta^3\text{He}$ values become comparable to the observations in all basins. With the exception of the Indian ocean, the simulated helium isotopic composition now appear globally quite reasonable, even if some discrepancies (classically attributed to coarse resolution models) remain:

- The overflow of the densest NADW formed in the Nordic Seas is poorly simulated [5,11,15,16] such that NADW ventilation does not penetrate below 3000m depth. Consequently, the Deep Western Boundary Current is too sluggish to maintain a realistic ^3He isotopic composition of newly formed NADW while it is transported to the south.
- The model failed to correctly reproduce the eastward propagation of the enriched ^3He plume in the deep ocean Pacific observed along the WOCE PO4 Section (Fig. 5), maintaining too high values close to the East Pacific Rise source.

The Indian Ocean is the only basin where the model failed to produce a realistic range of ^3He altogether, with all experiments largely exceeding the observations. The source function could be to blame, but the results obtained during the multimodel OCMIP2 project tend to indicate that this formulation of the source function is not inaccurate [12]. On the other hand, the deep overturning circulations of all our simulations are very weak in this basin ($<2\text{sv}$). This is far below all observational estimates: $27 \pm 10\text{Sv}$ [51], $12 \pm 3\text{Sv}$ [41], $11 \pm 3\text{Sv}$ [19], $23 \pm 3\text{Sv}$ [46]. This large discrepancy in the overturning circulation in the Indian Ocean is common to a large set of general circulation models [38]. In our simulations, it is unambiguously the main reason for the overestimation of the helium isotopic composition in this basin.

6 Conclusion

Having taken into account the experience gained during the OCMIP2 project, we have performed simulations with a new configuration of the OPA model in order to improve its deep ocean ventilation. Natural ^3He , with its large sensitivity to ocean circulation, proves a useful constraint for the evaluation of the validity of the simulated deep circulation, as large uncertainties remain in the estimations of ocean overturning derived from hydrographic data [50].

It was found that the control version of the model, with low vertical mixing, generated an unrealistically sluggish circulation that led to an overestimated ^3He isotopic composition. Including the parameterization with enhanced vertical mixing in the deep ocean provided a major improvement to the model's circulation. It is thus recommended to pursue this effort and to test some more sophisticated parameterizations, such those developed for representing the effect of tides on the topography [24].

Second, the inclusion of a geothermal forcing provided an additional—though modest—enhancement of the AABW circulation. However, its impact on simulated ^3He was substantial and brought the simulated tracer distributions in a close agreement with observations for most basins. This supports the notion that ^3He is a key oceanographic tracer, providing constraints independent of, and complementary to, hydrographic transport estimates. This additional information corroborates the suggestion that geothermal heating has a significant dynamical impact on the simulated circulation of our model [13] and, we expect, other ocean GCMs besides those where it has already been found [1,45,52]. Since it was found in Emile-Geay and Madec [13] that the inclusion of a realistic geothermal heat flow both improved the fit to both circulation and temperature field, ^3He is now the third observational constraint to be positively affected by this process in OPA. Taken together, these constraints strongly suggest that geothermal heating is indeed essential to abyssal dynamics.

The next step would be to carry out a similar analysis with different ocean GCMs, possibly including a broader suite of tracers to diversify the constraints and help discriminate between the most relevant physical processes and parameterizations. Using higher resolution models would also offer the opportunity to better simulate the detailed structure of the $\delta^3\text{He}$ distribution observed in the deep ocean and even allow to simulate other dynamical process that can affect the $\delta^3\text{He}$ distribution, such as entrainment and vertical pumping associated with the geothermal heat flux [28,49]. This will be left for future investigation.

References

1. Adcroft A, Scott J, Marotzke J (2001) Impact of geothermal heating on the global ocean circulation. *Geophys Res Lett* 28:1735–1738
2. Adkins JF, Ingersoll AP, Pasquero C (2005) Rapid climate change and conditional instability of the glacial deep ocean from the thermobaric effect and geothermal heating. *Q Sci Rev* 24:581–594
3. Beckmann A, Döscher R (1997) A method for improved representation of dense water spreading over topography in geopotential-coordinate models. *J Phys Oceanogr* 27:581–591
4. Blanke B, Delecluse P (1993) Variability of the tropical ocean simulated by a general circulation model with mixed layer-physics. *J Phys Oceanogr* 23:1363–1388
5. Böning CW, Holland WR, Bryan FO, Danabasoglu G, McWilliams JC (1995) An overlooked problem in model simulations of the thermohaline circulation and heat transport in the Atlantic Ocean. *J Clim* 8:515–523
6. Broecker WS, Peng TH (1982) Tracers in the sea, Lamont Doherty Geological Observatory. Palisades, New York, 690 pp
7. Bryan F (1987) Parameter sensitivity of primitive equation ocean general circulation models. *J Phys Oceanogr* 17:970
8. Craig H, Clarke WB, Beg MA (1975) Excess ^3He in deep water on the east Pacific rise. *Earth Planet Sci Lett* 26:125–132
9. Danabasoglu G, McWilliams JC, Gent PR (1994) The role of mesoscale tracer transports in global ocean circulation. *Science* 264:1123–1126
10. Duffy PB, Caldeira K, Selvaggi J, Hoffert MI (1997) Effects of subgrid-scale mixing parametrizations on simulated distributions of natural ^{14}C , temperature and salinity in a three-dimensional ocean general circulation model. *J Phys Oceanogr* 27:498–523
11. Dutay J-C, Bullister JL, Doney SC, Orr JC, Najjar R, Caldeira K, Campin J-M, Drange H, Follows M, Gao Y, Gruber N, Hecht MW, Ishida A, Joos F, Lindsay K, Madec G, Maier-Reimer E, Marshall JC,

- Matear RJ, Monfray P, Mouchet A, Plattner G-K, Sarmiento J, Schlitzer R, Slater R, Totterdell IJ, Weirig M-F, Yamanaka Y, Yool A (2002) Evaluation of ocean model ventilation with cfc-11: comparison of 13 global ocean models. *Ocean Model* 4:89–120
12. Dutay J-C, Jean-Baptiste P, Campin JM, Ishida A, Maier-Reimer E, Matear RJ, Mouchet A, Totterdell IJ, Yamanaka Y, Rodgers K, Madec G, Orr JC (2004) Evaluation of OCMIP-2 ocean model's deep circulation with mantle ^3He . *J Mar Syst* 48:15–36
 13. Emile-Geay J, Madec G (2009) Geothermal heating, diapycnal mixing, and the abyssal circulation. *Ocean Sci* 5:203–218
 14. England MH, Hirst AC (1997) Chlorofluorocarbon uptake in a world ocean model 2. Sensitivity to surface thermohaline forcing and subsurface mixing parameterizations. *J Geophys Res* 102:15709–15731
 15. England M, Holloway G (1998) Simulations of cfc content and water mass age in the deep north Atlantic. *J Geophys Res* 103:15885–15901
 16. England MH, Rahmstorf S (1999) Sensitivity of ventilation rates and radiocarbon uptake to subgrid-scale mixing in ocean models. *J Phys Oceanogr* 29:2802–2827
 17. Farley KA, Maier-Reimer E, Schlosser P, Broecker WS (1995) Constraints on mantle ^3He fluxes and deep-sea circulation from an oceanic general circulation model. *J Geophys Res* 100:3829–3839
 18. Ganachaud A (2003) Large-scale mass transports, water mass formation, and diffusivities from world ocean circulation experiment (WOCE) hydrographic data. *J Geophys Res* 108. doi:[10.1029/2002JC001565](https://doi.org/10.1029/2002JC001565)
 19. Ganachaud A, Wunsch C, Marotzke J, Toole J (2000) Meridional overturning and large-scale circulation of the Indian Ocean. *J Geophys Res* 105:26117–26134
 20. Gent PR, Willebrand J, McDougall TJ, McWilliams JC (1995) Parameterizing eddy-induced tracer transports in ocean circulation models. *J Phys Oceanogr* 25:463–474
 21. Gooose H, Campin JM, Fichefet T, Deleersnijder E (1997) Impact of sea-ice formation on the properties of Antarctic bottom water. *Ann Glaciol* 25:276–281
 22. Iudicone D, Madec G, Blanke B, Speich S (2008) The role of the southern ocean surface forcings and mixing in the global conveyor belt. *J Phys Oceanogr* 38:1357–1376
 23. Iudicone D, Speich S, Madec G, Blanke B (2008) The global conveyor belt from a southern ocean perspective. *J Phys Oceanogr* 38:1401–1425
 24. Jayne SR, Laurent LCS (2001) Parameterizing tidal dissipation over rough topography. *Geophys Res Lett* 28:811–814
 25. Jean-Baptiste P (1992) Helium-3 distribution in the deep world ocean: its relation to hydrothermal ^3He fluxes and to terrestrial heat budget. In: Consultants meeting on isotopes of noble gases as tracers in environmental studies, Vienna
 26. Joyce T, Warren B, Talley L (1986) The geothermal heating of the abyssal subarctic Pacific Ocean. *Deep Sea Res* 33(8):1003–1015
 27. Kamenkovich IV, Goodman PJ (2000) The dependence of AABW transport in the Atlantic on vertical diffusivity. *Geophys Res Lett* 27:3739–3742
 28. Lupton JE (1995) Hydrothermal plumes: near and far field. In: Humphris S, Zierenberg R, Mullineaux L, Thomson R (eds) *Seafloor hydrothermal systems: physical, chemical, biological, and geological interactions*. Geophysical Monograph 91. American Geophysical Union, Washington, DC, pp 317–346
 29. Lupton JE (1996) A far-field hydrothermal plume from Loihi Seamount. *Science* 272:976–979
 30. Lupton JE (1998) Hydrothermal helium plumes in the Pacific Ocean. *J Geophys Res* 103:15853–15868
 31. Lupton JE, Craig H (1981) A major helium-3 source at 15°S on the east pacific rise. *Science* 214:13–18
 32. Madec G, Imbard M (1996) A global ocean mesh to overcome the north pole singularity. *Clim Dyn* 12:381–388
 33. Madec G, Delecluse P, Imbard M, Lévy C (1998) Opa8.1 ocean general circulation model reference manual. Notes du pôle de Modélisation de l'IPSL 11
 34. Müller RD, Roest WR, Royer J-Y, Gahagan LM, Sclater JG (1997) Digital isochrons of the ocean floor. *J Geophys Res* 102(32):3211–3214
 35. Munk W, Wunsch C (1998) Abyssal recipes II: energetics of tidal and wind mixing. *Deep Sea Res* 45:1977–2010
 36. Naveira Garabato AC, Stevens DP, Watson AJ, Roether W (2007) Short-circuiting of the oceanic overturning circulation in the Antarctic Circumpolar Current. *Nature* 447(7141):194–197. doi:[10.1038/nature05832](https://doi.org/10.1038/nature05832)
 37. Orsi AH, Johnson GC, Bullister JL (1999) Circulation, mixing, and production of antarctic bottom water. *Prog Oceanogr* 43:55–109
 38. Palmer MD, Naveira Garabato AC, Stark JD, Hirschi JJ-M, Marotzke J (2007) The influence of diapycnal mixing on quasi-steady overturning states in the Indian Ocean. *J Phys Oceanogr* 37:2290–2304

39. Paul A, Schäfer-Neth C (2003) Modeling the water masses of the Atlantic Ocean at the Last Glacial Maximum. *Paleoceanography* 18(3):1058. doi:[10.1029/2002PA000783](https://doi.org/10.1029/2002PA000783)
40. Rahmstorf S (2002) Ocean circulation and climate during the past 120,000 years. *Nature* 419:207–214
41. Robbins PE, Toole JM (1997) The dissolved silica budget as a constraint on the meridional overturning circulation of the Indian Ocean. *Deep Sea Res I* 44:879–906
42. Roullet G, Madec G (2000) Salt conservation, free surface and varying volume: a new formulation for ocean GCMs. *J Geophys Res* 105:23927–23942
43. Schmitz WJ Jr (1995) On the interbasin-scale thermohaline circulation. *Rev Geophys* 33:151–173
44. Schlösser P, Bullister JL, Fine R, Jenkins WJ, Key R, Lupton J, Roether W, Smethie W (2001) Transformation and age of water masses. In: Siedler G, Church J, Gould J (eds) *Ocean circulation and climate*. Academic Press, San Diego
45. Scott J, Marotzke J, Adcroft A (2001) Geothermal heating and its influence on the meridional overturning circulation. *J Geophys Res* 106:1–14
46. Sloyan BM, Rintoul SR (2001) The southern ocean limb of global deep overturning circulation. *J Phys Oceanogr* 31:143–173
47. Srinivasan A, Top Z, Schlosser P, Hohmann R, Iskandarani M, Olson DB, Lupton JE, Jenkins WJ (2004) Mantle ^3He distribution and deep circulation in the Indian Ocean. *J Geophys Res* 109:C06012. doi:[10.1029/2003JC002028](https://doi.org/10.1029/2003JC002028)
48. Stein CA, Stein S (1992) A model for the global variation in oceanic depth and heat flow with lithospheric age. *Nature* 359:123–129
49. Stommel H (1982) Is the south Pacific helium-3 plume dynamically active?. *Earth Planet Sci Lett* 61:63–67
50. Talley LD, Reid JL, Robbins PE (2003) Data-based meridional overturning streamfunctions for the global ocean. *J Clim* 16:3213–3226
51. Toole JM, Warren BA (1993) A hydrographic section across the subtropical south Indian Ocean. *Deep Sea Res I* 40:1973–2019
52. Urakawa LS, Hasumi H (2009) A remote effect of geothermal heat on the global thermohaline circulation. *J Geophys Res* 114:C07016. doi:[10.1029/2008JC005192](https://doi.org/10.1029/2008JC005192)
53. Visbeck M (2002) Climate—the ocean's role in Atlantic climate variability. *Science* 297(5590):2223–2224
54. Visbeck M (2007) Concept oceanography: power of pull. *Nature* 447:383. doi:[10.1038/447383a](https://doi.org/10.1038/447383a)
55. Wanninkhof R (1992) Relationship between wind speed and gas exchange over the ocean. *J Geophys Res* 97:7373–7382
56. Weber SL, Drijfhout SS, Abe-Ouchi A, Crucifix M, Eby M et al (2007) The modern and glacial overturning circulation in the Atlantic ocean in PMIP coupled model simulations. *Clim Past* 3:51–64
57. Wijffels SE, Toole JM, Bryden HL, Fine RA, Jenkins WJ, Bullister JL (1996) The water masses and circulation at 10N in the Pacific. *Deep Sea Res* 43:501–544
58. Wunsch C, Ferrari R (2004) Vertical mixing, energy, and the general circulation of the oceans. *Annu Rev Fluid Mech* 36:281–314